

Update on Atmospheric Neutrinos<sup>1</sup>

M. C. Gonzalez-Garcia

Instituto de Física Corpuscular - C.S.I.C./Universidad de Valencia. Spain  
andInstituto de Física Teórica, Universidade Estadual Paulista  
Rua Pamplona 145, 01405-900 São Paulo, Brazil

E-mail: concha.gonzalez@uv.es

## ABSTRACT

I summarize here the results of a global fit to the full data set corresponding to 535 days of data of the Super-Kamiokande experiment as well as to all other experiments in order to compare the two most likely solutions to the atmospheric neutrino anomaly in terms of oscillations in the  $\nu_\mu \rightarrow \nu_\tau$  and  $\nu_\mu \rightarrow \nu_s$  channels.

## 1. Introduction

Atmospheric showers are initiated when primary cosmic rays hit the Earth's atmosphere. Secondary mesons produced in this collision, mostly pions and kaons, decay and give rise to electron and muon neutrino and anti-neutrino fluxes<sup>2</sup>. There has been a long-standing anomaly between the predicted and observed  $\nu_\mu = \nu_e$  ratio of the atmospheric neutrino fluxes<sup>3</sup>. Although the absolute individual  $\nu_\mu$  or  $\nu_e$  fluxes are only known to within 30% accuracy, different authors agree that the  $\nu_\mu = \nu_e$  ratio is accurate up to a 5% precision. In this resides our confidence on the atmospheric neutrino anomaly (ANA), now strengthened by the high statistics sample collected at the Super-Kamiokande experiment<sup>4</sup>. The most likely solution of the ANA involves neutrino oscillations. In principle we can invoke various neutrino oscillation channels, involving the conversion of  $\nu_\mu$  into either  $\nu_e$  or  $\nu_\tau$  (active-active transitions) or the oscillation of  $\nu_\mu$  into a sterile neutrino  $\nu_s$  (active-sterile transitions). This last case is especially well-motivated theoretically, since it constitutes one of the simplest ways to reconcile<sup>5</sup> the ANA with other puzzles in the neutrino sector such as the solar neutrino problem as well as the LSND result<sup>6</sup> and the possible need for a few eV mass neutrino as the hot dark matter in the Universe<sup>7</sup>.

The main aim of this talk is to compare the  $\nu_\mu \rightarrow \nu_\tau$  and the  $\nu_\mu \rightarrow \nu_s$  transitions using the new sample corresponding to 535 days of the Super-Kamiokande data.

---

<sup>1</sup>To Appear in Proceeding of the RINGBERG EUROCONFERENCE - NEW TRENDS IN NEUTRINO PHYSICS Ringberg Castle, Tegernsee, Germany, 24 - 29 May 1998

This analysis uses the latest improved calculations of the atmospheric neutrino fluxes as a function of zenith angle, including the muon polarization effect and taking into account a variable neutrino production point<sup>8</sup>.

## 2. Atmospheric Neutrino Oscillation Probabilities

The expected neutrino event number both in the absence and the presence of oscillations can be written as:

$$N = N_{\nu} + N_e; \quad N_e = N_{ee} + N_{\nu e}; \quad (1)$$

where

$$N = n_t T \int_0^z \frac{d^2}{dE d(\cos \theta)} (\nu; \cos \theta; E) P \frac{d}{dE} \sigma(E) dE d(\cos \theta) dh; \quad (2)$$

and  $P$  is the oscillation probability of  $\nu_i \rightarrow \nu_j$  for given values of  $E$ ;  $\cos \theta$  and  $h$ , i.e.,  $P = P(\nu_i \rightarrow \nu_j; E; \cos \theta; h)$ . In the case of no oscillations, the only non-zero elements are the diagonal ones, i.e.  $P = 1$  for all  $i = j$ .

Here  $n_t$  is the number of targets,  $T$  is the experiment's running time,  $E$  is the neutrino energy and  $\nu$  is the flux of atmospheric neutrinos of type  $\nu = \nu_e, \nu_\mu, \nu_\tau$ ;  $E$  is the neutrino energy and  $\sigma(E)$  is the detection efficiency for such charged lepton;  $\sigma$  is the neutrino-nucleon interaction cross section, and  $\theta$  is the angle between the vertical direction and the incoming neutrinos ( $\cos \theta = 1$  corresponds to the downcoming neutrinos). In Eq. (2),  $h$  is the slant distance from the production point to the sea level for  $\nu$ -type neutrinos with energy  $E$  and zenith angle  $\theta$ . Finally,  $dh$  is the slant distance distribution which is normalized to one<sup>8</sup>.

The neutrino fluxes, in particular in the sub-GeV range, depend on the solar activity. In order to take this fact into account in Eq. (2), a linear combination of atmospheric neutrino fluxes  $\nu^{max}$  and  $\nu^{min}$ , which correspond to the most active Sun (solar maximum) and quiet Sun (solar minimum) respectively, is used.

For definiteness we assume a two-flavor oscillation scenario, in which the neutrino oscillates into another flavour either  $\nu_e \rightarrow \nu_\mu$ ,  $\nu_e \rightarrow \nu_\tau$  or  $\nu_\mu \rightarrow \nu_\tau$ . The Schrodinger evolution equation of the  $\nu_X$  (where  $X = e, \mu$  or  $\tau$  sterile) system in the matter background for neutrinos is given by

$$\begin{aligned} i \frac{d}{dt} \nu_X &= \begin{pmatrix} H_{\nu_X} & H_{\nu_X} \\ H_{\nu_X} & H_{\nu_X} \end{pmatrix} \nu_X; & (3) \\ H_{\nu_X} &= V + \frac{m^2}{4E} \cos 2\theta_X; & H_{\nu_X} = V_X + \frac{m^2}{4E} \cos 2\theta_X; \\ H_{\nu_X} &= \frac{m^2}{4E} \sin 2\theta_X \end{aligned}$$

where

$$V = V = \frac{P}{M} \frac{2G_F}{2} \left( \frac{1}{2} Y_n \right); \quad V_s = 0$$

$$V_e = \frac{P}{M} \frac{2G_F}{2} \left( Y_e - \frac{1}{2} Y_n \right)$$

Here  $G_F$  is the Fermi constant,  $P$  is the matter density at the Earth,  $M$  is the nucleon mass, and  $Y_e$  ( $Y_n$ ) is the electron (neutron) fraction. We define  $m^2 = m_2^2 - m_1^2$  in such a way that if  $m^2 > 0$  ( $m^2 < 0$ ) the neutrino with largest muon-like component is heavier (lighter) than the one with largest X-like component. For anti-neutrinos the signs of potentials  $V_X$  should be reversed. We have used the approximate analytic expression for the matter density profile in the Earth obtained in ref. <sup>16</sup>. In order to obtain the oscillation probabilities  $P$  we have made a numerical integration of the evolution equation. The probabilities for neutrinos and anti-neutrinos are different because the reversal of sign of matter potential. Notice that for the  $\mu \rightarrow e$  case there is no matter effect while for the  $\mu \rightarrow \tau$  case we have two possibilities depending on the sign of  $m^2$ . For  $m^2 > 0$  the matter effects enhance neutrino oscillations while depress antineutrino oscillations, whereas for the other sign ( $m^2 < 0$ ) the opposite holds. The same occurs also for  $\mu \rightarrow e$ . Although in the latter case one can also have two possible signs, we have chosen the most usually assumed case where the muon neutrino is heavier than the electron neutrino, as it is theoretically more appealing. Notice also that, as seen later, the allowed region for this sign is larger than for the opposite, giving the most conservative scenario when comparing with the present limits from CHOOZ.

### 3. Atmospheric Neutrino Data Fits

Here I describe our fit method to determine the atmospheric oscillation parameters for the various possible oscillation channels, including matter effects for both  $\mu \rightarrow e$  and  $\mu \rightarrow \tau$  channels. The steps required in order to generate the allowed regions of oscillation parameters were given in ref. <sup>1</sup>. I will comment only that when combining the results of the experiments we do not make use of the double ratio,  $R_{\mu e} = R_{\mu e}^{MC}$ , but instead we treat the e and  $\tau$ -like data separately, taking into account carefully the correlation of errors. It is well-known that the double ratio is not well suited from a statistical point of view due to its non-Gaussian character. Thus, following ref. <sup>17</sup> we define the  $\chi^2$  as

$$\chi^2 = \sum_{I,J}^X (N_I^{data} - N_I^{theory})^2 \frac{1}{(N_I^{data} + N_I^{theory})} + \sum_{J} (N_J^{data} - N_J^{theory})^2; \quad (4)$$

where  $I$  and  $J$  stand for any combination of the experimental data set and event-type considered, i.e.,  $I = (A; \nu)$  and  $J = (B; \nu)$  where,  $A; B$  stands for Frejus, Kamikande sub-GeV, IMB, ... and  $\nu = e; \tau$ . In Eq. (4)  $N_I^{theory}$  is the predicted number of events

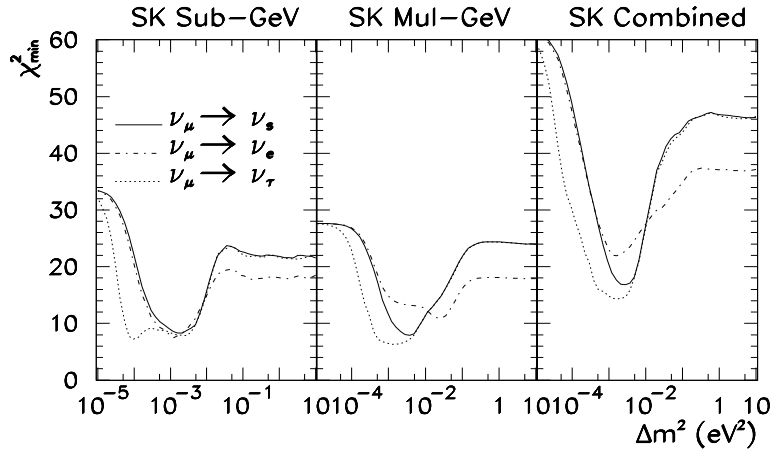


Fig. 1.  $\chi^2_{\text{min}}$  for fixed  $m^2$  versus  $m^2$  for each oscillation channel for Super-Kamiokande sub-GeV and multi-GeV data, and for the combined sample. Since the minimum is always obtained close to maximum mixing the curves for  $\nu_\mu \rightarrow \nu_e$  for both signs of  $m^2$  coincide.

calculated from Eq. (1) whereas  $N_I^{\text{data}}$  is the number of observed events. In Eq. (4)  $\chi^2_{\text{data}}$  and  $\chi^2_{\text{theory}}$  are the error matrices containing the experimental and theoretical errors respectively. They can be written as

$$\chi^2_{\text{IJ}} = \begin{pmatrix} A & A;B \\ A;B & B \end{pmatrix} \quad (5)$$

where  $(A;B)$  stands for the correlation between the  $\nu_\mu$ -like events in the A-type experiment and  $\nu_\mu$ -like events in B-type experiment, whereas  $(A)$  and  $(B)$  are the errors for the number of  $\nu_\mu$  and  $\nu_\mu$ -like events in A and B experiments, respectively.

We compute  $(A;B)$  as in ref. <sup>17</sup>. A detailed discussion of the errors and correlations used in the analysis can be found in Ref. <sup>1</sup>. We have conservatively ascribed a 30% uncertainty to the absolute neutrino flux, in order to generously account for the spread of predictions in different neutrino flux calculations. Next we minimize the  $\chi^2$  function in Eq. (4) and determine the allowed region in the  $\sin^2 2\theta - m^2$  plane, for a given confidence level, defined as,

$$\chi^2 \leq \chi^2_{\text{min}} + 4.61 \quad (9.21) \quad \text{for } 90 \text{ (99)\% C.L.} \quad (6)$$

In Fig. 1 we plot the minimum  $\chi^2$  (minimized with respect to  $\sin^2 2\theta$ ) as a function of  $m^2$ . Notice that for large  $m^2 > 0.1 \text{ eV}^2$ , the  $\chi^2$  is nearly constant. This happens because in this limit the contribution of the matter potential in Eq. (4) can be neglected with respect to the  $m^2$  term, so that the matter effect disappears and moreover, the oscillation effect is averaged out. In fact one can see that in this range we obtain nearly the same  $\chi^2$  for the  $\nu_\mu \rightarrow \nu_e$  and  $\nu_\mu \rightarrow \nu_\tau$  cases. For very small  $m^2 < 10^{-4} \text{ eV}^2$ , the situation is opposite, namely the matter term dominates and we obtain a better fit for the  $\nu_\mu \rightarrow \nu_e$  channel, as can be seen by comparing the  $\nu_\mu \rightarrow \nu_e$  curve of the Super-Kamiokande sub-GeV data (dotted curve in the left panel of Fig. 1) with the  $\nu_\mu \rightarrow \nu_e$

and  $\theta_{13}$  curves in the left panel of Fig. 1). For extremely small  $m^2 < 10^4$   $\text{eV}^2$ , values of  $\theta_{13}$  is quite large and approaches a constant, independent of oscillation channel, as in the no-oscillation case. Since the average energy of Super-Kamiokande multi-GeV data is higher than the sub-GeV one, we find that the limiting  $m^2$  value below which  $\theta_{13}$  approaches a constant is higher, as seen in the middle panel. Finally, the right panel in Fig. 1 is obtained by combining sub and multi-GeV data. A last

Table 1. Minimum value of  $\theta_{13}$  and the best fit point for each oscillation channel and for different data sets. For  $\theta_{13}$ 's the minimum  $\theta_{13}$  is practically independent of the sign of  $m^2$  as the minimum is located at maximum mixing angle.

Experiment		$\theta_{13}$	$\theta_{13}^s$	$\theta_{13}^e$
Super-Kamiokande sub-GeV	$m_{\text{min}}^2$ ( $10^3 \text{eV}^2$ ) $\sin^2 2\theta_{13}$	7:1 0:11 1:0	8:2 1:9 1:0	7:3 1:2 0:97
Super-Kamiokande multi-GeV	$m_{\text{min}}^2$ ( $10^3 \text{eV}^2$ ) $\sin^2 2\theta_{13}$	6:3 1:5 0:97	7:9 3:5 1:0	10:8 24:7 0:72
Super-Kamiokande Combined	$m_{\text{min}}^2$ ( $10^3 \text{eV}^2$ ) $\sin^2 2\theta_{13}$	14:3 1:6 1:0	16:8 2:6 1:0	21:8 1:5 0:97
All experiments Combined	$m_{\text{min}}^2$ ( $10^3 \text{eV}^2$ ) $\sin^2 2\theta_{13}$	47:2 2:9 1:0	48:6 3:5 1:0	48:6 3:0 0:99

point worth commenting is that for the  $\theta_{13}^e$  case in the sub-GeV sample there are two almost degenerate values of  $m^2$  for which  $\theta_{13}^e$  attains a minimum while for the multi-GeV case there is just one minimum at  $1.5 \cdot 10^3 \text{eV}^2$ . Finally in the third panel in Fig. 1 we can see that by combining the Super-Kamiokande sub-GeV and multi-GeV data we have a unique minimum at  $1.6 \cdot 10^3 \text{eV}^2$ .

#### 4. Results for the Oscillation Parameters

The results of our fit of the Super-Kamiokande sub-GeV and multi-GeV atmospheric neutrino data are given in Fig. 2. In this figure we give the allowed region of oscillation parameters at 90 and 99% CL. One can notice that the matter effects are similar for the upper right and lower right panels because matter effects enhance the oscillations for neutrinos in both cases. In contrast, in the case of  $\theta_{13}^s$  with  $m^2 < 0$  the enhancement occurs only for anti-neutrinos while in this case the effect of matter suppresses the conversion in  $\nu_\mu$ 's. Since the yield of atmospheric neutrinos is bigger than that of anti-neutrinos, clearly the matter effect suppresses the overall conversion probability. Therefore we need in this case a larger value of the vacuum mixing angle, as can be seen by comparing the left and right lower panels in Fig. 2.

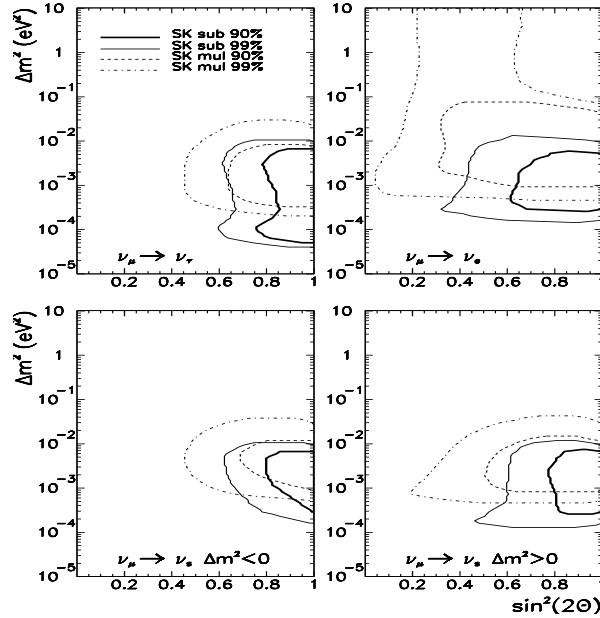


Fig. 2. Allowed regions of oscillation parameters for Super-Kamiokande for the different oscillation channels as labeled in the figure. In each panel, we show the allowed regions for the sub-G eV data at 90 (thick solid line) and 99 % C.L. (thin solid line) and the multi-G eV data at 90 (dashed line) and 99 % C.L. (dot-dashed line).

Notice that in all channels where matter effects play a role the range of acceptable  $m^2$  is shifted towards larger values, when compared with the  $\nu_\mu \rightarrow \nu_\tau$  case. This follows from looking at the relation between mixing in vacuo and in matter. In fact, away from the resonance region, independently of the sign of the matter potential, there is a suppression of the mixing inside the Earth. As a result, there is a lower cut in the allowed  $m^2$  value, and it lies higher than what is obtained in the data fit for the  $\nu_\mu \rightarrow \nu_\tau$  channel.

It is also interesting to analyse the effect of combining the Super-Kamiokande sub-G eV and multi-G eV atmospheric neutrino data. Comparing the results obtained with 535 days given in the table above with those obtained with 325 days of Super-Kamiokande<sup>1</sup> we see that the allowed region is relatively stable with respect to the increased statistics. However, in contrast to the case for 325.8 days, now the  $\nu_\mu \rightarrow \nu_\tau$  channel is as good as the  $\nu_\mu \rightarrow \nu_e$ , when only the sub-G eV sample is included, with a clear Super-Kamiokande preference for the  $\nu_\mu \rightarrow \nu_\tau$  channel. As before, the combined sub-G eV and multi-G eV data prefers the  $\nu_\mu \rightarrow \nu_X$ , where  $X = \tau$  or sterile, over the  $\nu_\mu \rightarrow \nu_e$  solution.

To conclude this section I now turn to the predicted zenith angle distributions for the various oscillation channels. As an example we take the case of the Super-Kamiokande experiment and compare separately the sub-G eV and multi-G eV data with what is predicted in the case of no-oscillation (thick solid histogram) and in all

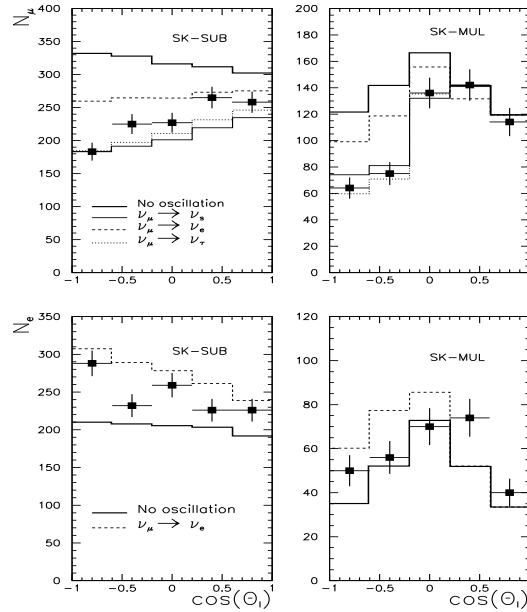


Figure 3: Angular distribution for Super-Kamiokande electron-like and muon-like sub-G eV and multi-G eV events together with our prediction in the absence of oscillation (dot-dashed) as well as the prediction for the best fit point for  $\theta_s$  (solid line),  $\theta_e$  (dashed line) and  $\theta_s$  (dotted line) channels. The error displayed in the experimental points is only statistical.

oscillation channels for the corresponding best fit points obtained for the combined sub and multi-G eV data analysis performed above (all other histograms). This is shown in Fig. 3.

It is worthwhile to see why the  $\theta_e$  channel is bad for the Super-Kamiokande multi-G eV data by looking at the upper right panel in Fig. 3. Clearly the zenith distribution predicted in the no oscillation case is very much in disagreement with the data. In the presence of  $\theta_e$  oscillations the asymmetry in the distribution is much smaller than in the  $\theta_s$  or  $\theta_s$  channels, as seen from the figure. Also since the best fit point for  $\theta_s$  occurs at  $\sin(2\theta) = 1$ , the corresponding distributions are independent of the sign of  $m^2$ .

## 5. Atmospheric versus Accelerator and Reactor Experiments

I now turn to the comparison of the information obtained from the analysis of the atmospheric neutrino data presented above with the results from reactor and accelerator experiments as well as the sensitivities of future experiments. For this purpose I present the results obtained by combining all the experimental atmospheric neutrino data from various experiments<sup>3</sup>. In Fig. 4 we show the combined information obtained

from our analysis of all atmospheric neutrino data involving vertex-contained events and compare it with the constraints from reactor experiments such as KamLAND, Bugey, and CHOOZ<sup>9</sup>, and the accelerator experiments such as CDHSW, CHORUS, and NOMAD<sup>10</sup>. We also include in the same figure the sensitivities that should be attained at the future long-baseline experiments now under discussion.

The first important point is that from the upper-right panel of Fig. 4 one sees that the CHOOZ reactor<sup>9</sup> data already exclude completely the allowed region for the  $\nu_e \rightarrow \nu_s$  channel when all experiments are combined at 90% CL. The situation is different if only the combined sub-GeV and multi-GeV Super-Kamiokande are included. In such a case the region obtained is not completely excluded by CHOOZ at 90% CL. Present accelerator experiments are not very sensitive to low  $m^2$  due to their short baseline. As a result, for all channels other than  $\nu_e \rightarrow \nu_s$  the present limits on neutrino oscillation parameters from CDHSW, CHORUS and NOMAD<sup>10</sup> are fully consistent with the region indicated by the atmospheric neutrino analysis. Future long baseline (LBL) experiments have been advocated as a way to independently check the ANA. Using different tests such long-baseline experiments now planned at KEK (K2K)<sup>11</sup>, Fermilab (MINOS)<sup>12</sup> and CERN (ICARUS<sup>13</sup>, NOE<sup>14</sup> and OPERA<sup>15</sup>) would test the pattern of neutrino oscillations well beyond the reach of present experiments. These tests are the following:  $\nu_e$  appearance searches, NC=CC ratio which measures  $\frac{(NC=CC)_{near}}{(NC=CC)_{far}}$ , and the muon disappearance or  $CC_{near}=CC_{far}$  test. The second test can potentially discriminate between the active and sterile channels, i.e.  $\nu_e \rightarrow \nu_s$  and  $\nu_e \rightarrow \nu_s$ . However it cannot discriminate between  $\nu_e \rightarrow \nu_s$  and the no-oscillation hypothesis. In contrast, the last test can probe the oscillation hypothesis itself. Notice that the sensitivity curves corresponding to the disappearance test labelled as KEK-SK Disappearance at the lower panels of Fig. 4 are the same for the  $\nu_e \rightarrow \nu_s$  and the sterile channel since the average energy of KEK-SK is too low to produce a tau-lepton in the far detector. In contrast the MINOS experiment has a higher average initial neutrino energy and it can see the tau's. Although in this case the exclusion curves corresponding to the disappearance test are in principle different for the different oscillation channels, in practice, however, the sensitivity plot is dominated by the systematic error. As a result discriminating between  $\nu_e \rightarrow \nu_s$  and  $\nu_e \rightarrow \nu_s$  would be unlikely with the Disappearance test.

In summary we find that the regions of oscillation parameters obtained from the analysis of the atmospheric neutrino data on vertex-contained events cannot be fully tested by the LBL experiments, when the Super-Kamiokande data are included in the fit for the  $\nu_e \rightarrow \nu_s$  channel as can be seen clearly from the upper-left panel of Fig. 4. One might expect that, due to the upward shift of the  $m^2$  indicated by the fit for the sterile case, it would be possible to completely cover the corresponding region of oscillation parameters. This is the case for the MINOS disappearance test. But in general since only the disappearance test can discriminate against the no-oscillation hypothesis, and this test is intrinsically weaker due to systematics, we find

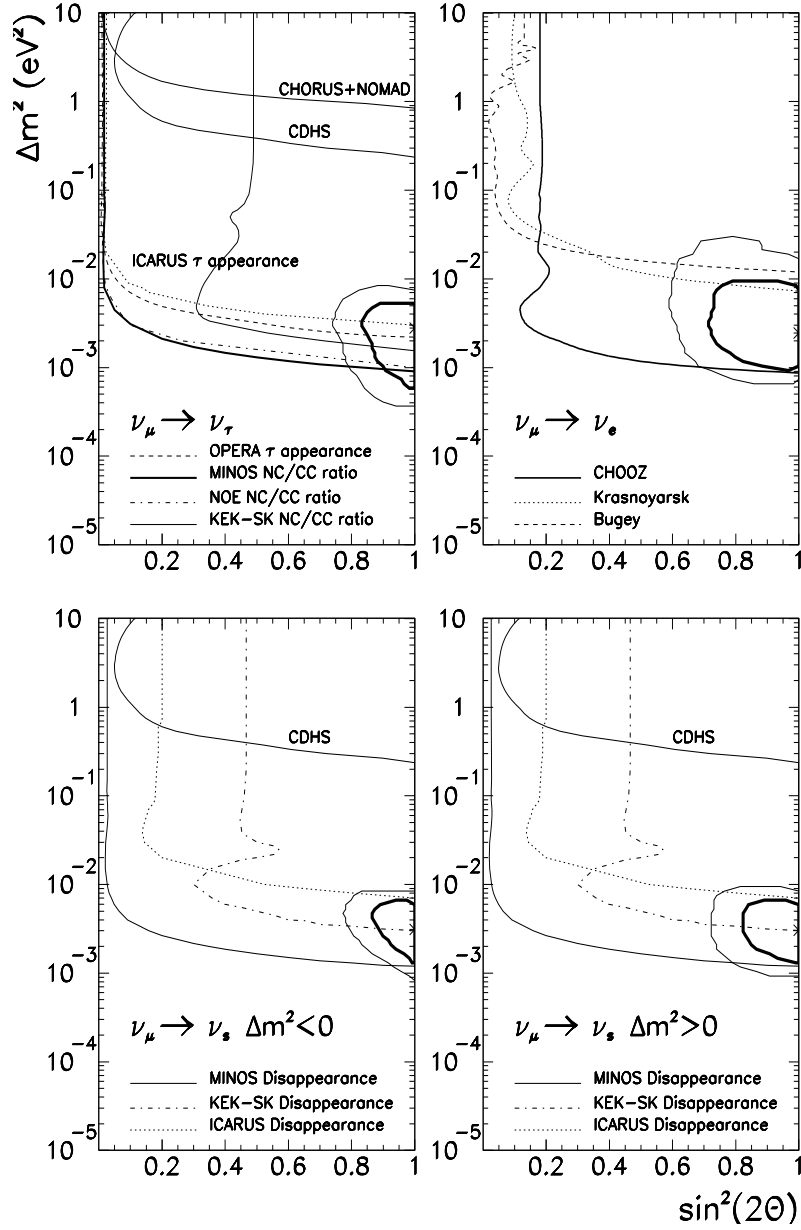


Fig. 4. Allowed oscillation parameters for all experiments combined at 90 (thick solid line) and 99 % CL (thin solid line) for each oscillation channel as labeled in the figure. We also display the expected sensitivity of the present accelerator and reactor experiments as well as to future long-baseline experiments in each channel. The best fit point is marked with a star.

that also for the sterile case most of the LBL experiments can not completely probe the region of oscillation parameters indicated by the atmospheric neutrino analysis. This is so irrespective of the sign of  $m^2$ : the lower-left panel in Fig. 4 shows the  $\nu_s$  channel with  $m^2 < 0$  while the  $\bar{\nu}_s$  case with  $m^2 > 0$  is shown in the lower-right panel.

I am very grateful to the Instituto de Física Teórica of the Universidade Estadual Paulista where these proceedings were written for its kind hospitality during my visit. This work was supported by DGICYT under grant PB 95-1077, by CICYT under grant AEN 96-1718, and by Fundação de Amparo a Pesquisa do Estado de São Paulo.

1. Based on the work by M. C. Gonzalez-Garcia, H. Nunokawa, O. L. G. Peres, T. Stanev and J. W. F. Valle, Phys. Rev. D 58, 033004 (1998), and M. C. Gonzalez-Garcia, H. Nunokawa, O. L. G. Peres, and J. W. F. Valle, FTUV/98-56, IFIC/98-57.
2. For a review, see for e.g. T. K. Gaisser, F. Halzen and T. Stanev, Phys. Rep. 258, 174 (1995) and references therein.
3. NUSEX Collaboration, M. Aglietta et al., Europhys. Lett. 8, 611 (1989); Frejus Collaboration, Ch. Berger et al., Phys. Lett. B 227, 489 (1989); IMB Collaboration, D. Casper et al., Phys. Rev. Lett. 66, 2561 (1991); R. Becker-Szendy et al., Phys. Rev. D 46, 3720 (1992); Kamokande Collaboration, H. S. Hirata et al., Phys. Lett. B 205, 416 (1988) and Phys. Lett. B 280, 146 (1992); Kamokande Collaboration, Y. Fukuda et al., Phys. Lett. B 335, 237 (1994); Soudan Collaboration, W. W. M. Allison et al., Phys. Lett. B 391, 491 (1997).
4. Super-Kamokande Collaboration: Y. Fukuda et al, hep-ex/9805006; Super-Kamokande Collaboration: Y. Fukuda et al, hep-ex/9803006; See also Talk by Chang Kee Jung in these Proceedings.
5. See talks by J. W. F. Valle, R. Mohapatra, C. Giunti and S. M. Bilenky, in these Proceedings.
6. C. Athanassopoulos, Phys. Rev. Lett. 77, 3082 (1996); Phys. Rev. C 54, 2708 (1996); J. E. Hill, Phys. Rev. Lett. 75, 2654 (1995).
7. R. Shaefer and Q. Sha, Nature 359, 199 (1992); E. L. Wright et al., Astrophys. J. 396, L13 (1992); A. Klypin et al., ibid. 416, 1 (1993); J. R. Primack et al., Phys. Rev. Lett. 74, 2160 (1995).
8. V. Agrawal et al., Phys. Rev. D 53, 1314 (1996); L. V. Volkova, Sov. J. Nucl. Phys. 31, 784 (1980); T. K. Gaisser and T. Stanev, Phys. Rev. D 57 1977 (1998).
9. G. S. Vidyakin et al., JETP Lett. 59, 390 (1994); B. Achkar et al., Nucl. Phys. B 424, 503 (1995); CHOOZ Collaboration, M. Apollonio et al., Phys. Lett. B 420 397 (1998).
10. CDHSW Collaboration, F. Dydak et al., Phys. Lett. B 134, 281 (1984); CHORUS Collaboration, E. Eskut et al., Nucl. Instrum. Meth. A 401, 7 (1997); NOMAD Collaboration, J. Altegoer et al., Nucl. Instrum. Meth. A

404, 96 (1998).

11. KEK-SK Collaboration, Proposal for Participation in Long-Baseline Neutrino Oscillation Experiment E362 at KEK, W. Gajewski et al. (unpublished).
12. MINOS Collaboration, D. Michael et al., Proceedings of XVI International Workshop on Weak Interactions and Neutrinos, Capri, Italy, 1997, edited by G. Fiori et al., [Nucl. Phys. B (Proc. Suppl.) 66 (1998) 432].
13. ICARUS Collaboration, A. Rubia et al., Proceedings of XVI International Workshop on Weak Interactions and Neutrinos, Capri, Italy, 1997, edited by G. Fiori et al., [Nucl. Phys. B (Proc. Suppl.) 66 (1998) 436].
14. NOE Collaboration, M. Ambrosio et al., Nucl. Instr. Meth. A 363, 604 (1995);
15. OPERA Collaboration, A. Ereditato et al., Proceedings of XVI International Workshop on Weak Interactions and Neutrinos, Capri, Italy, 1997, edited by G. Fiori et al., [Nucl. Phys. B (Proc. Suppl.) 66 (1998) 423].
16. E. Lisi and D. Montanino, Phys. Rev. D 56, 1792 (1997).
17. G. L. Fogli, E. Lisi, Phys. Rev. D 52, 2775 (1995); G. L. Fogli, E. Lisi and D. Montanino, Phys. Rev. D 49, 3626 (1994); Astrop. Phys. 4, 177 (1995); G. L. Fogli, E. Lisi, D. Montanino and G. Scioscia Phys. Rev. D 55, 485 (1997).